

Passenger Mobility Prediction via Representation Learning for Dynamic Directed and Weighted Graph

YUANDONG WANG, School of Computer Science and Engineering, Beihang University, China
 HONGZHI YIN* and TONG CHEN, School of Information Technology and Electrical Engineering,
 The University of Queensland, AU
 CHUNYANG LIU and BEN WANG, Didichuxing, China
 TIANYU WO*, School of Computer Science and Engineering, Beihang University, China
 JIE XU, School of Computing, University of Leeds, UK

In recent years, ride-hailing services have been increasingly prevalent as they provide huge convenience for passengers. As a fundamental problem, the timely prediction of passenger demands in different regions is vital for effective traffic flow control and route planning. As both spatial and temporal patterns are indispensable passenger demand prediction, relevant research has evolved from pure time series to graph-structured data for modeling historical passenger demand data, where a snapshot graph is constructed for each time slot by connecting region nodes via different relational edges (e.g., origin-destination relationship, geographical distance, etc.). Consequently, the spatiotemporal passenger demand records naturally carry dynamic patterns in the constructed graphs, where the edges also encode important information about the directions and volume (i.e., weights) of passenger demands between two connected regions. However, existing graph-based solutions fail to simultaneously consider those three crucial aspects of dynamic, directed, and weighted (DDW) graphs, leading to limited expressiveness when learning graph representations for passenger demand prediction. Therefore, we propose a novel spatiotemporal graph attention network, namely **Gallat** (Graph prediction with **all** attention) as a solution. In Gallat, by comprehensively incorporating those three intrinsic properties of DDW graphs, we build three attention layers to fully capture the spatiotemporal dependencies among different regions across all historical time slots. Moreover, the model employs a subtask to conduct pretraining so that it can obtain accurate results more quickly. We evaluate the proposed model on real-world datasets, and our experimental results demonstrate that Gallat outperforms the state-of-the-art approaches.

CCS Concepts: • **Information systems** → **Data mining**; *Enterprise applications*; *Spatial-temporal systems*; • **Computing methodologies** → **Neural networks**;

Additional Key Words and Phrases: Dynamic Graph; Representation Learning; Passenger Demand Prediction

ACM Reference Format:

Yuandong Wang, Hongzhi Yin*, Tong Chen, Chunyang Liu, Ben Wang, Tianyu Wo*, and Jie Xu. 2021. Passenger Mobility Prediction via Representation Learning for Dynamic Directed and Weighted Graph. 1, 1 (January 2021), 24 pages. <https://doi.org/10.1145/nnnnnnn.nnnnnnn>

*Corresponding author.

Authors' addresses: Yuandong Wang, School of Computer Science and Engineering, Beihang University, Beijing, China, wangyd@act.buaa.edu.cn; Hongzhi Yin*, Tong Chen, School of Information Technology and Electrical Engineering, The University of Queensland, Brisbane, AU, {h.yin1,tong.chen}@uq.edu.au; Chunyang Liu; Ben Wang, Didichuxing, Beijing, China, {liuchunyang.wangben}@didiglobal.com; Tianyu Wo*, School of Computer Science and Engineering, Beihang University, Beijing, China, woty@act.buaa.edu.cn; Jie Xu, School of Computing, University of Leeds, Leeds, UK, J.Xu@leeds.ac.uk.

Permission to make digital or hard copies of all or part of this work for personal or classroom use is granted without fee provided that copies are not made or distributed for profit or commercial advantage and that copies bear this notice and the full citation on the first page. Copyrights for components of this work owned by others than ACM must be honored. Abstracting with credit is permitted. To copy otherwise, or republish, to post on servers or to redistribute to lists, requires prior specific permission and/or a fee. Request permissions from permissions@acm.org.

© 2021 Association for Computing Machinery.

XXXX-XXXX/2021/1-ART \$15.00

<https://doi.org/10.1145/nnnnnnn.nnnnnnn>

1 INTRODUCTION

Transportation plays a very important role in our daily lives. In 2018, commuters in Beijing spend about 112 minutes behind the wheel on average every day. With the prominent development of technologies like GPS and mobile Internet, various ride-hailing applications have emerged to provide drivers and passengers with more convenience, such as Didi, Lyft and Uber. For all ride-hailing platforms, analyzing and predicting the real-time passenger demand is the key to high-quality services, which has recently started to attract considerable research attention.

Initially, the majority of studies [35, 40, 47] treat passenger demand prediction as a time series prediction problem which predicts the number of passenger demands in an arbitrary location during a given time period. However, such prediction paradigm only considers the origin of each passenger's trip, and neglects the destination information. To account for this important aspect in passenger demand prediction, recent research [4, 11] defines it as an Origin-Destination Matrix Prediction (ODMP) problem. In ODMP, each time slot has its own OD matrix, where the element indexed by (i, j) describes the travel demand from region i to region j . In this regard, tensor factorization models [6, 11] and convolutional neural networks (CNNs) [20, 24] can be conveniently adopted to extract latent representations from the OD matrices to support prediction. Additionally, ODMP not only estimates the number of passenger demands within the target area, but also foresees where these demands go, making it easier for ride-hailing companies to coordinate travel resources (i.e., vehicles) to maximize customer satisfaction and business revenue.

More recently, research on passenger demand has introduced a new perspective by modelling the traffic data as graphs where different regions are viewed as nodes. Compared with OD matrices, graph-structured data is able to uniform various heterogeneous information to help boost the prediction accuracy. For instance, two region nodes can be connected by different edges representing specific relationships, e.g., origin-destination relationship in a time slot [31], geographical association (e.g., adjacency regions) [41], and even functionality similarity by comparing their point-of-interest distributions [5]. With the recent advances in graph neural networks (GNNs) [10, 16, 38], GNN-based models have emerged and yielded state-of-the-art performance in a wide range of passenger demand prediction and traffic modelling tasks [3, 5, 31, 41]. On one hand, GNN-based models are capable of mining the complex and heterogeneous relationships between regions, thus thoroughly capturing the latent properties of each region to allow for accurate demand prediction. On the other hand, GNN-based models are versatile as they generalize the convolutional operations in CNNs to the non-Euclidean graph topologies without the need for conversion into OD matrices at each time slot.

When modelling traffic data as graphs, a common practice is to construct a snapshot graph for each time slot. Consequently, this results in three major intrinsic properties of such graph-structured data, i.e., the constructed graphs are *dynamic*, *directed*, and *weighted*. In our paper, this notion is referred to as dynamic, directed, and weighted (DDW) graphs, which contain both the spatial and temporal information across regions. From a temporal perspective, DDW graphs are time-sensitive due to complex real-life situations (e.g., peak hour traffic, special events, etc.), making it non-trivial to fully capture their dynamics. For every DDW snapshot graph, two regions are linked via an edge if there are observed trip orders between them, thus allowing GNN-based models to capture signals of spatial passenger flows. However, on top of that, in an origin-destination relationship, the edge between two region nodes should be directional. For example, a central business district tends to have substantially more inbound traffic flows than outbound flows during morning peak hours. Also, as the volume of passenger demand varies largely among different routes, those origin-destination edges should preserve such information as their weights. Unfortunately, existing methods tend to oversee these two important edge properties, leading to severe information

loss. For instance, graph-structured data is used to extract temporal features of each region [5], but neither the direction nor the volume of passengers is captured by the constructed graphs. Though [41] considers the weights of edges when learning representations for each region nodes, it simply treats the passenger flows between two nodes from both directions equally without distinguishing their semantics.

Meanwhile, as a widely reported issue in passenger demand research [11, 41, 46], the geographically imbalanced distribution of trip orders inevitably incurs sparsity issues within the constructed graphs. Due to varied locations and public resource allocations, the observable passenger flows from/to some regions (e.g., rural areas) are highly scarce. While most existing studies seek solutions by gathering side information from multiple data sources (e.g., point-of-interests [5, 40], weather [22, 41], real-time events [35], etc.), it is impractical to assume the constant availability and high quality of such auxiliary data. Hence, it further highlights the necessity of fully capturing the latent patterns and comprehensively modelling the information within DDW graphs constructed from historical trip orders.

To this end, we propose Gallat, namely **Graph prediction with all attention**, which is a novel spatiotemporal graph neural network for passenger demand prediction. Specifically, having the self-attention as its main building block, Gallat consists of three main parts: the spatial attention layer, the temporal attention layer, and the transferring attention layer. In the spatial attention layer, we learn each region node's representation by discriminatively aggregating information from its three types of neighbor nodes with attention mechanism. To be specific, we innovatively define forward and backward neighborhoods respectively for its outbound and inbound travel records to distinguish the different semantics of two directions. The geographical neighborhood is also defined for each node to gather information from nearby regions and help alleviate data sparsity. In the temporal attention layer, we deploy a multi-channel self-attention mechanism to retrieve important contextual information from the history, which is then used to augment the learned node representations for demand prediction in the next time slot. With the generated representation of each node from the first two layers, we firstly predict the total number of passenger demands in each region, and then distribute it to all possible destination regions via a transferring probability generated in the final transferring attention layer. By taking advantages of the attention mechanism, our model Gallat is highly expressive, and is able to capture the heterogeneous connectivity among regions to yield optimal prediction performance.

The main contributions of this work are as follows:

- We investigate passenger demand from the perspective of DDW graphs, with a comprehensive take on modelling the dynamic, directed, and weighted properties within the passenger flow data simultaneously.
- We propose a novel spatiotemporal graph neural network named Gallat, which is an inductive solution to representation learning on DDW graphs for passenger demand prediction.
- Extensive experiments are conducted on two real-world datasets, and the results demonstrate the superior effectiveness of our proposed model.

2 PRELIMINARIES

In this section, we provide key definitions and formally define the passenger mobility prediction problem.

DEFINITION 1. *Time Slot.* We evenly partition the time into a sequence of T slots, which are represented as $t \in \{1, 2, \dots, T\}$. The interval between any two consecutive slots is constant. For example, we can divide a day into 24 one-hour time slots.

DEFINITION 2. Node. The entire area of interest like a city is divided into n non-overlapping regions. Each region is regarded as a node, and the node set of the specific city can be denoted as $\mathcal{V} = \{v_1, v_2, \dots, v_n\}$. Following [11, 41, 47], we determine regions by evenly dividing a whole area into grids according to their longitudes and latitudes. Then, we calculate the physical distance between each pair of nodes using their central coordinates, which is stored in an adjacency matrix \mathbf{R} . Every element $r_{i,j} \in \mathbf{R}$ represents the geographical distance between node v_i and node v_j .

DEFINITION 3. Dynamic, Directed, and Weighted graph. In a time slot, the passenger mobility in the region of interest can be modeled as interactions between nodes. Given a fixed region node set $\mathcal{V} = \{v_1, v_2, \dots, v_n\}$, we use $e_{ij} = (v_i \rightarrow v_j, g_{ij})$ to denote the directional edge from v_i to v_j , where g_{ij} is the weight of the edge. In our paper, each g_{ij} is directly defined as the number of passenger demands from region v_i to v_j in a specific time slot. If there are no trip orders from v_i to v_j , then $g_{ij} = 0$ denotes a non-existing edge. We use a sequence of adjacency matrices $\{\mathbf{G}_t\}_{t=1}^T = \{\mathbf{G}_1, \mathbf{G}_2, \dots, \mathbf{G}_T\}$ to represent all DDW graphs in all T time slots where $\mathbf{G}_t = \{g_{ij}^t\}_{i,j=1}^n \in \mathbb{N}^{n \times n}$.

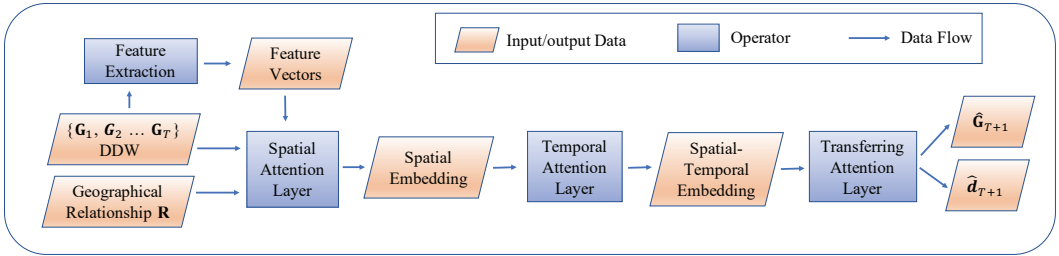


Fig. 1. **The overview of Gallat model.** This figure depicts the key components and data flow of the model.

Here, we formulate the passenger mobility prediction problem as follows:

PROBLEM 1. Passenger Mobility Prediction. For a fixed region node set \mathcal{V} , given all DDW snapshot graphs $\{\mathbf{G}_t\}_{t=1}^T$ in the past T time slots and the geographical relationship \mathbf{R} among nodes, we define passenger mobility prediction as a DDW graph prediction problem, which aims to predict the DDW snapshot graph \mathbf{G}_{T+1} in the next time slot.

3 SOLUTION

In this section, we present the detail of our model Gallat, a spatiotemporal attention network for passenger demand prediction. Figure 1 depicts the overview of our proposed model. With the DDW graph sequence $\{\mathbf{G}_t\}_{t=1}^T$ and the geographical relationship \mathbf{R} as the model input, the feature extraction module generates the feature vector \mathbf{v}_i^t for node v_i at the t -th time slot. Then, we define a spatial attention layer to learn a spatial representation (i.e., embedding) for every node at time t by aggregating information from nodes within three distinct types of spatial neighborhoods. Afterwards, all nodes' representations will be fed into a temporal attention layer, which updates its current embedding with the captured temporal dependencies among its historical embeddings. In our transferring attention layer, we first calculate the total number of outbound passenger demands departing from each region and the transferring probability between every pair of nodes with the current embeddings, and then use the resulted probabilities to map each region's total passenger demands to the corresponding destination regions, which will compose the information in the next DDW snapshot graph \mathbf{G}_{T+1} .

Table 1. Notations

Notation	Description
t	a time slot
T	the total number of time slots in a sequence
\mathcal{V}	a node set
v_i	a node
\mathbf{V}_t	the matrix of all nodes' feature vectors at t
\mathbf{v}_i^t	the feature vector of node v_i at time slot t , $\mathbf{v}_i^t \in \mathbf{V}_t$
\mathbf{R}	an adjacency matrix of nodes' geographical relationship
$r_{i,j}$	the geographical distance between node v_i and v_j , $r_{i,j} \in \mathbf{R}$
\mathbf{G}_t	an adjacency matrix of DDW graphs at time slot t
g_{ij}^t	the passenger demand between node v_i and v_j , $g_{ij}^t \in \mathbf{G}_t$
$\Psi_i^t, \Phi_i^t, \Theta_i$	the sets of node v_i 's forward, backward and geographical neighbors' indexes at time slot t
L	the threshold of the distance to determine the size of v_i 's geographical neighborhood
\mathbf{M}_t	the matrix of all nodes' representation vectors
m_i^t	node v_i 's representation vector at time slot t , $m_i^t \in \mathbf{M}_t$
ψ_{ij}^t, ϕ_{ij}^t and θ_{ij}^t	attentive weights between three different neighbors of v_i and v_j
a_j^t, b_j^t, c_j	pre-weights of different kinds of neighbors
P	the number of historical time slots considered in each channel
\mathcal{S}	a channel's sequence of \mathbf{M}_t , $\mathcal{S} \in \{\mathcal{S}_1, \mathcal{S}_2, \mathcal{S}_3, \mathcal{S}_4\}$
$\mathbf{M}_{\mathcal{S}}$	the aggregated representation of the sequence \mathcal{S}
\mathbf{M}_T'	the final representation of time slot T
\mathbf{V}_{T+1}	the matrix that stores n nodes' features at time slot $T + 1$
$\mathbf{d}_{T+1}, \mathbf{G}_{T+1}$	the outbound passenger demands and the snapshot of DDW graph at time slot $T + 1$
$\hat{\mathbf{d}}_{T+1}, \hat{\mathbf{G}}_{T+1}$	the predicted results of \mathbf{d}_{T+1} and \mathbf{G}_{T+1}
\hat{d}_i, \hat{g}_{ij}	the elements of $\hat{\mathbf{d}}_{T+1}$ and $\hat{\mathbf{G}}_{T+1}$
q_{ij}	the transferring probability between node v_i and v_j
$\mathcal{L}, \mathcal{L}_d, \mathcal{L}_o$	loss functions
η_d, η_o	the weights of loss functions
$\mathbf{a}, \mathbf{w}, \mathbf{b}$	the weights to learn
d, d_e, d_v	the dimensions of feature vectors during $\{1, \dots, t\}$, embedding layers and feature vectors at time slots $T + 1$
$\mathbf{W}, \mathbf{W}_s, \mathbf{W}_a, \mathbf{W}'_a, \mathbf{W}^K_{\mathcal{S}}, \mathbf{W}^Q_{\mathcal{S}}, \mathbf{W}^V_{\mathcal{S}}, \mathbf{W}^K_{\mathcal{S}}, \mathbf{W}^Q_{\mathcal{S}}, \mathbf{W}^V_{\mathcal{S}}$	the weight matrices to learn

3.1 Feature Extraction

Given a region node v_i , we first construct its feature vector by merging relevant information from multiple sources. Specifically, the feature vector $\mathbf{v}_i^t \in \mathbb{R}^d$ for node v_i at time t is the concatenation of feature embeddings from all feature fields (e.g., weather, day of the week, etc.):

$$\mathbf{v}_i^t = \mathbf{v}_i^{t,1} \oplus \dots \oplus \mathbf{v}_i^{t,f} \oplus \dots \oplus \mathbf{v}_i^{t,F}, \quad (1)$$

where F is the total number of feature fields, and \oplus denotes the concatenation operation. Note that $\mathbf{v}_i^{t,f}$ can be either a dense embedding vector for categorical features (e.g., node ID) or a real-valued number for continuous features (e.g., temperature). As such, for each snapshot DDW graph \mathbf{G}_t , we can obtain the features of all n nodes $\mathbf{V}_t = \{\mathbf{v}_i^t\}_{i=1}^n$ to support subsequent computations. In our experiments, a node v_i 's feature vector \mathbf{v}_i^t is the concatenation of its row, column, out degree, in degree in the graph \mathbf{G}_t , as well as the embeddings of the node ID, time slot t and the corresponding day of a week.

3.2 Spatial Attention Layer

In this section, inspired by the inductive graph representation learning approach [10], we learn a latent representation \mathbf{m}_i for node v_i at time t by effectively aggregating the features of its neighbors. Different from [10] which only focuses on a single type of neighbors, we define three types of neighbors in DDW graphs, namely forward neighbors and backward neighbors based on passenger mobility, and geographical neighbors based on physical locations. We make the statistics of real-world data in Beijing during one month. As shown in Figure 2, we summarize the mean values of a non-peak time slot (3:00am) and a peak one (9:00am). It can be seen that the forward neighbors and backward neighbors exhibit different distributions in the same time slot and the same type of neighbors also show different distributions at different time slots. Hence, it is meaningful to distinguish the forward and backward neighbors. We first give the definition of forward and backward neighborhoods for each node as follows.

3.2.1 Forward Neighborhood. If there is at least one demand starting from region node v_i and ending at v_j , i.e., $g_{ij}^t > 0$, then v_j is a forward neighbor of v_i . For node v_i , its forward neighborhood at an arbitrary time slot t is a set of node indexes defined as:

$$\Psi_i^t = \{j | g_{ij}^t > 0, g_{ij}^t \in \mathbf{G}_t\}. \quad (2)$$

3.2.2 Backward Neighborhood. Similarly, if there is at least one demand starting from region node v_j and ending at v_i , then v_j is a backward neighbor of v_i . For node v_i , at an arbitrary time slot t , we can obtain a set of its backward neighbors' indexes via:

$$\Phi_i^t = \{j | g_{ji}^t > 0, g_{ji}^t \in \mathbf{G}_t\}. \quad (3)$$

According to Eq.(2) and Eq.(3), it is worth mentioning that the numbers of different nodes' forward and backward neighbors are asymmetrical and time-dependent. The rationale of defining forward and backward neighborhoods is that the characteristics of each region are not only determined by its intrinsic features, but also affected by its interactions with other regions. Intuitively, if more trip orders are observed between nodes v_i and v_j at time t , they are more likely to possess a higher semantic affinity in that time slot. Hence, by propagating the representations of node v_i 's neighbors to itself, the properties from closely related nodes can complement its original representation, thus producing an updated embedding of node v_i with enriched contexts. Moreover, when modelling passenger demands as DDW graphs, the direction of an edge carries crucial information about different mobility patterns, and indicates varied functionalities of regions. For example, it is common to see a residential area has many people travelling to the central business district for work during the morning rush hours; while in the evening when people return home from work, a large passenger flow may be observed in the reverse direction. Hence, for two linked nodes, unlike [41] that treats the passenger demands from both directions equally, we define the forward and backward neighbors to distinguish their semantics and allow them to contribute differently to the resulted node embedding.

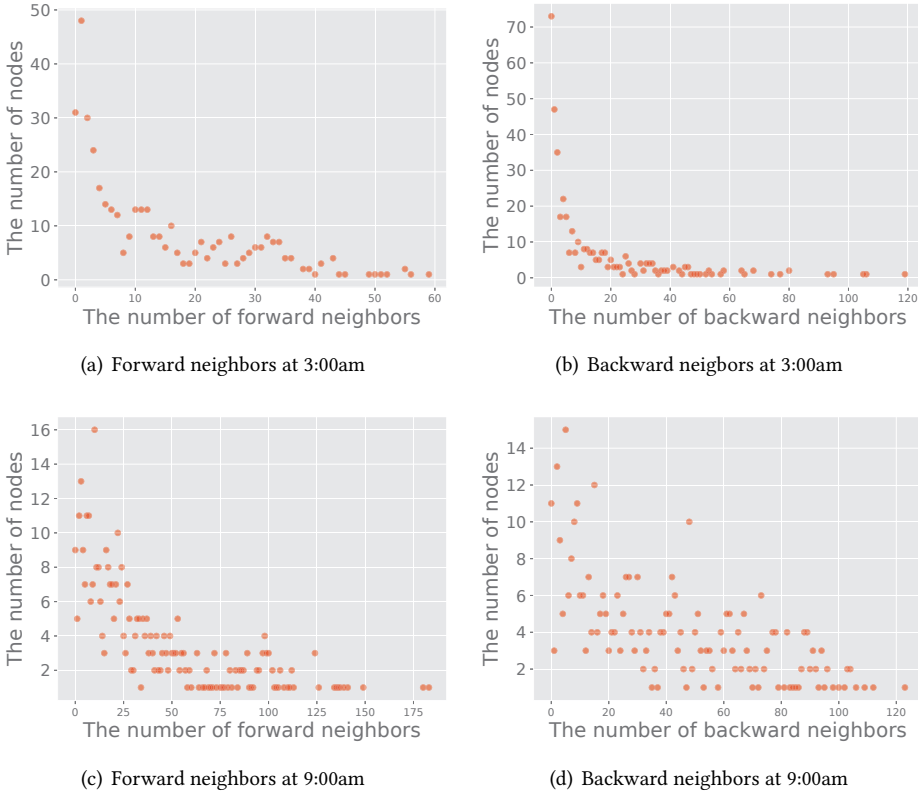


Fig. 2. The forward and backward neighbors' distribution at different time slots

Apart from that, we also capture the information from geographically connected regions in the spatial attention layer. Geographical neighbors of region node v_i are nodes that are physically close to it, which are constant across T time slots.

3.2.3 Geographical Neighborhood. As Definition 2 states, the nodes in our DDW graphs are manually-divided and non-overlapping grids with all pairwise geographical relationship \mathbf{R} . For a node v_i , its static geographical neighborhood Θ_i is formulated as:

$$\Theta_i = \{j | r_{i,j} \leq L, r_{i,j} \in \mathbf{R}\}, \tag{4}$$

where L is a threshold of the distance to determine the size of v_i 's neighborhood. A node's geographical neighbors are important for its embedding. Intuitively, being the geographical neighbors of v_i , the nodes in Θ_i are more likely to own similar inner properties as v_i , thus leading to close distributions of passenger demands. For example, if node v_i and v_j are adjacent and located in a sparsely populated suburb, then both of them are likely to have fewer demands. The geographical neighbors also help alleviate the data sparsity problem. For example, if a node has very few forward and backward neighbors at a specific time t , the features of its geographical neighbors will become a key supplementary information resource to ensure the learning of discriminative node representation.

It is worth mentioning that these three kinds of neighborhoods carry different information from both semantic and geographical perspectives. They need to be transferred to the next step of the

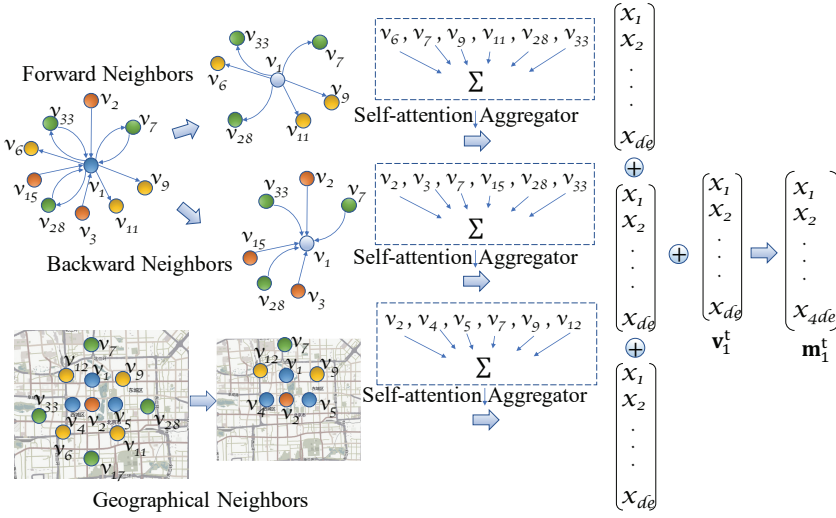


Fig. 3. **The illustration of spatial attention layer.** This figure describes the neighborhood definition and aggregation in spatial attention layer. Σ means calculating the attention weighted and element-wise mean of the neighbors' feature vectors, and \oplus represents the concatenation of vectors.

model separately so we utilize the attention-based aggregator to gather information within each kinds of neighborhood and concatenate the aggregating results of them in the following steps.

3.2.4 Attention-based Aggregator. With three types of node neighborhoods defined, we devise an attention-based aggregator to merge the respective node information within Ψ_i^t , Φ_i^t and Θ_i . Taking the feature vectors of all nodes in the neighbor sets, i.e., $\{v_j | j \in \Psi_i^t\}$, $\{v_j | j \in \Phi_i^t\}$ and $\{v_j | j \in \Theta_i\}$ as the input, the attention-based aggregator fuses them into a unified vector representation m_i^t for each node v_i at time t . Before detailing our attention-based aggregator for node embedding, we first briefly introduce the naive form of aggregator introduced in [10], which is originally designed for static graphs without any direction or weight information on edges:

$$\mathbf{m}_i^t = \sigma\left(\mathbf{W} \cdot (\mathbf{v}_i^t \oplus \text{Aggregate}\{v_j^t | j \in \mathcal{N}\})\right), \quad (5)$$

where m_i^t represents the resulted embedding vectors of node v_i , \mathbf{W} is the weight matrix to learn, and σ is the nonlinear *Sigmoid* activation function. To aggregate the information passed from neighbor nodes using the aggregation function $\text{Aggregate}(\cdot)$, the GraphSAGE proposed in [10] creates a paradigm that allows the model to sample and aggregate a fixed number of neighbors \mathcal{N} . However, GraphSAGE uniformly samples a relatively small number of neighbors, which treats all neighbor nodes evenly and neglects their varied importance of a node's neighbors. Also, for a popular region, only sampling a small subset of its neighbors will lead to severe information loss. Consequently, the learned embedding of v_i will likely fail to pay sufficient attention to closely related neighbors, and be vulnerable to the noise from semantically irrelevant nodes. In addition, as [10] simply assumes there is only one homogeneous type of neighborhood relationship in a graph (i.e., \mathcal{N}), Eq.(5) is unable to simultaneously handle information within the heterogeneous neighbors we have defined for passenger demand prediction. In light of this, we propose an attention-based aggregation scheme to discriminatively select important nodes via learned attentive weights, which

also extends Eq.(5) to our three heterogeneous neighborhood sets:

$$\mathbf{m}_i^t = \mathbf{W}_s \mathbf{v}_i^t \oplus \sum_{j \in \Psi_i^t} \psi_{ij}^t \mathbf{W}_s \mathbf{v}_j^t \oplus \sum_{j \in \Phi_i^t} \phi_{ij}^t \mathbf{W}_s \mathbf{v}_j^t \oplus \sum_{j \in \Theta_i^t} \theta_{ij}^t \mathbf{W}_s \mathbf{v}_j^t, \quad (6)$$

where $\mathbf{W}_s \in \mathbb{R}^{d_e \times d}$ is a shared weight matrix that projects all feature vectors onto the same d_e dimensional embedding space. Notably, the specific *Aggregate*(\cdot) function we adopt is the weighted sums of node information within Ψ_i^t , Φ_i^t , and Θ_i^t , respectively. ψ_{ij}^t , ϕ_{ij}^t and θ_{ij}^t are the attentive weights between nodes v_i and v_j in the corresponding neighborhoods. In this attention layer, we focus on mining the fine-grained pairwise importance from the neighbor node to the target node. Hence, we employ the self-attention calculation of GAT [38] in Eq.(7) which is designed for graph node representation learning and would learn a more expressive representation for each node. To compute the attentive weights, we firstly define a shared attention network denoted by *AttentionNet*(\cdot, \cdot). *AttentionNet*(\cdot, \cdot) produces a scalar that quantifies the semantic affinity between nodes v_i and v_j using their features. Take one arbitrary node pair (v_i, v_j) at time t as an example, then *AttentionNet*($\mathbf{v}_i^t, \mathbf{v}_j^t$) is calculated as follows:

$$\text{AttentionNet}(\mathbf{v}_i, \mathbf{v}_j) = \mu(\mathbf{a}^\top (\mathbf{W}_a \mathbf{v}_i^t \oplus \mathbf{W}_a \mathbf{v}_j^t)), \quad (7)$$

where μ represents the *LeakyReLU* function that applies nonlinearity, $\mathbf{W}_a \in \mathbb{R}^{d_e \times d}$ is the learnable weight matrix, $\mathbf{a} \in \mathbb{R}^{2d_e \times 1}$ is the project weight that maps the concatenated vector to a scalar output. Then, we compute ψ_{ij}^t , ϕ_{ij}^t and θ_{ij}^t by applying *softmax* [27] to normalize all the attention scores between v_i and its forward, backward, and geographical neighbors:

$$\begin{aligned} \psi_{ij}^t &= \frac{\exp(\text{AttentionNet}(\mathbf{v}_i^t, a_j^t \mathbf{v}_j^t))}{\sum_{k \in \Psi_i^t} \exp(\text{AttentionNet}(\mathbf{v}_i^t, a_k^t \mathbf{v}_k^t))}, \\ \phi_{ij}^t &= \frac{\exp(\text{AttentionNet}(\mathbf{v}_i^t, b_j^t \mathbf{v}_j^t))}{\sum_{k \in \Phi_i^t} \exp(\text{AttentionNet}(\mathbf{v}_i^t, b_k^t \mathbf{v}_k^t))}, \\ \theta_{ij}^t &= \frac{\exp(\text{AttentionNet}(\mathbf{v}_i^t, c_j \mathbf{v}_j^t))}{\sum_{k \in \Theta_i^t} \exp(\text{AttentionNet}(\mathbf{v}_i^t, c_k \mathbf{v}_k^t))}, \end{aligned} \quad (8)$$

which enforces $\sum_{j \in \Psi_i^t} \psi_{ij}^t = \sum_{j \in \Phi_i^t} \phi_{ij}^t = \sum_{j \in \Theta_i^t} \theta_{ij}^t = 1$ and thus can be viewed as three probability distributions over the corresponding type of neighborhoods. The attention network is shared across the computations for all three neighborhoods. In Eq.(8), it is worth noting that, before being fed into the attention network, every neighbor node of v_i is weighted by a factor a , b and c for the forward, backward, and geographical neighborhood, respectively. Next, we explain the rationale of involving these weights in the computation of Eq.(8) and present the details of three pre-weighted functions for generating the weights a , b and c .

3.2.5 Pre-weighted Functions. The core idea behind our pre-weighted functions is to timely help sense the sparsity of the data and provide additional prior knowledge for the subsequent attention-based information aggregation. This is achieved by taking advantage of the observed weights on each DDW graph \mathbf{G}_t and the geographical relationship \mathbf{R} . Given the target node v_i , for any of its forward, backward or geographical neighbor v_j in Ψ_i^t , Φ_i^t or Θ_i^t , we derive three statistics-driven pre-weighted functions to compute the corresponding weight for v_j , i.e., a_j^t , b_j^t or

c_j :

$$\begin{aligned} a_j^t &= \frac{g_{ij}}{\sum_{j \in \Psi_i^t} g_{ij} + \epsilon}, \quad g_{ij} \in \mathbf{G}_t, \\ b_j^t &= \frac{g_{ji}}{\sum_{j \in \Phi_i^t} g_{ji} + \epsilon}, \quad g_{ji} \in \mathbf{G}_t, \\ c_j &= \frac{1}{\sum_{j \in \Theta_i} \frac{1}{r_{ij}}}, \quad r_{ij} \in \mathbf{R}, \end{aligned} \quad (9)$$

where ϵ is a small additive term in case the denominator is 0 (i.e., $\Psi_i^t = \emptyset$ or $\Phi_i^t = \emptyset$ in highly sparse data). As suggested by Eq.(9), the weights a_j^t and b_j^t reflect v_j 's intensity of passenger demands at time t . Therefore, the attention weights ψ_{ij}^t and ϕ_{ij}^t obtained in Eq.(8) is not only dependent on the semantic similarity between node features \mathbf{v}_i^t and \mathbf{v}_j^t , but also the real-time popularity of neighbor region node v_j at time t . Besides, motivated by Harmonic mean, the geographical weighting factor c_j essentially assigns larger weights to region nodes that are geographically closer to the target node v_i . As such, by coupling the pre-weighted functions with our attention-based aggregator, the embedding \mathbf{m}_i^t generated with Eq.(6) is an expressive blend of its inner properties and the characteristics of three distinct neighborhoods.

3.3 Temporal Attention Layer

So far, we can obtain a set of embeddings $\{\mathbf{m}_i^t\}_{i=1}^n \in \mathbb{R}^{4d_e}$ for all regions in each snapshot DDW graph \mathbf{G}_t . Specifically, for each time slot t , we use a feature matrix $\mathbf{M}_t = [\mathbf{m}_1^t, \mathbf{m}_2^t, \dots, \mathbf{m}_n^t]^\top \in \mathbb{R}^{n \times 4d_e}$ to vertically stack all n node embeddings at time t . Hence, for the DDW graph sequence $\{\mathbf{G}_t\}_{t=1}^T$, we can obtain T time-varying feature matrices $\{\mathbf{M}_t\}_{t=1}^T$ to represent the DDW graphs at corresponding time slots. For the current time slot T , since \mathbf{M}_T only carries the spatial information within the T -th DDW graph. To account for the dynamics within our DDW graphs, we develop a temporal attention layer to firstly capture the sequential dependencies among the learned representations in $\{\mathbf{M}_t\}_{t=1}^T$, and generate a spatiotemporal representation \mathbf{M}'_T for predicting the passenger demand in the next time slot. Obviously, a straightforward approach is to gather information from P most recent and consecutive DDW graphs, i.e., $\{\mathbf{M}_t\}_{t=T-P+1}^T$. However, in real-life scenarios, for the DDW graph at time T , only DDW graphs from time slots that are temporally close to T will exploit similar characteristics. In contrast, if there is a relatively big time gap between two DDW graphs, their characteristics will vary significantly, e.g., the traffic flow in the central business district will be much lower during midnight than in the morning. As a result, merely using consecutive time slots can introduce a large amount of noise when learning the spatiotemporal DDW graph representation \mathbf{M}'_T .

On this occasion, as Figure 4 shows, we design a multi-channel structure to capture the temporal patterns among different DDW graphs. To enhance the capability of learning useful information from historical DDW graphs, we infuse the periodicity within passenger demands into the temporal attention layer. Specifically, apart from the DDW graph sequence $\{\mathbf{M}_t\}_{t=T-P+1}^T$, we derive three periodical sequences to augment the long-term temporal information about the DDW graph at time T . First, we collect P historical DDW graphs from the same time slot of each day. For example, if we divide each day into 24 1-hour slots, then we can collect DDW graphs from the same 8:00–8:59 am slot from P consecutive days. Mathematically, we represent such sequence as $\mathcal{S}_1 = \{\mathbf{M}_t | t = T - lp + 1, p \in [1, P]\}$, where l is the number of time slots in a day ($l = 24$ in our case), and $P \leq \lfloor \frac{T}{l} \rfloor$. Similarly, to leverage the close contexts in directly adjacent time slots, we consider two periodical sequences for T 's prior and subsequent time slots (i.e., $T - 1$ and $T + 1$), which results

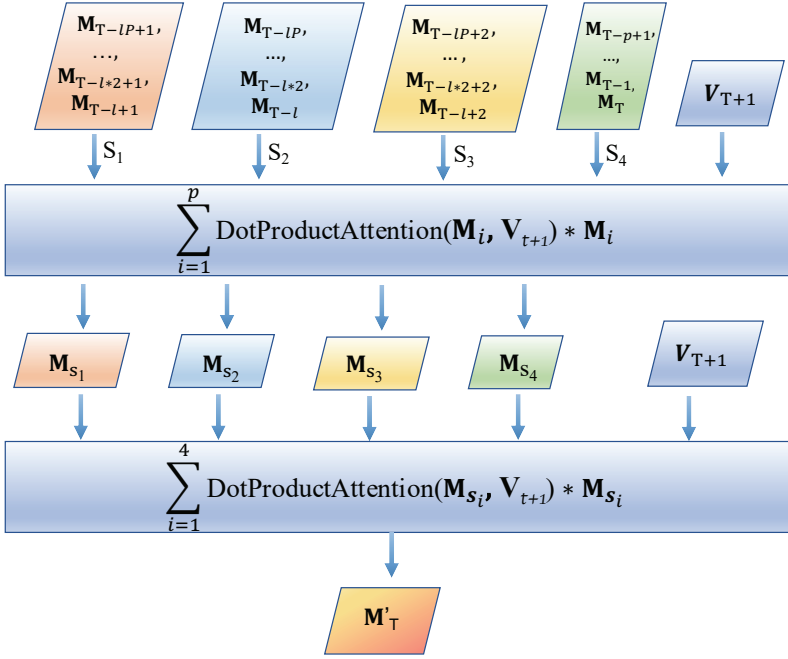


Fig. 4. **The architecture of temporal attention layer.** The temporal attention layer utilizes dot product attention mechanism to capture the dynamic property of DDW via four channels.

in $S_2 = \{M_t | t = T - lp, p \in [1, P]\}$ and $S_3 = \{M_t | t = T - lp + 2, p \in [1, P]\}$, respectively. The non-periodical sequence $S_4 = \{M_t\}_{t=T-p+1}^T$ is also used to capture short-term passenger demand fluctuations.

Correspondingly, we build our temporal attention layer with four channels to attentively aggregate the information within sequences S_1, S_2, S_3 , and S_4 :

$$M_S = \sum_{M_t \in S} \varrho \left(\frac{V_{T+1} W_S^Q \cdot (M_t W_S^K)^\top}{\sqrt{4d_e}} \right) \cdot M_t W_S^V, S \in \{S_1, S_2, S_3, S_4\} \quad (10)$$

where ϱ represents the row-wise *softmax* function. $W_S^K, W_S^V \in \mathbb{R}^{4d_e \times 4d_e}$ and $W_S^Q \in \mathbb{R}^{d_v \times 4d_e}$ are query, key and value weight matrices dedicated each channel S . $V_{T+1} = [v_1^{T+1}, v_2^{T+1}, \dots, v_n^{T+1}]^\top \in \mathbb{R}^{n \times d_v}$ is the feature matrix that stores n nodes' features at time $T + 1$. Each feature $v \in \mathbb{R}^{d_v}$ is generated with the same process as in Eq.(1). Note that $d_v \leq d$ because some features for time slot $T + 1$ might be unavailable at the current time T (e.g., the number of trip orders), and are hence excluded. Specifically, we formulate Eq.(10) with the notion of scaled dot product attention [37] which is different from the self-attention in Eq.(7). In this attention layer, we are more concerned on capturing the graph-level association in the time domain. To more efficiently and effectively compute an attentive feature matrix for the current graph, we adopt the scaled dot-product attention in Eq.(10). The rationale is that, the row-wise *softmax* first produces an $n \times n$ attention matrix A , where the i -th row $\{a_{ij}\}_{j=1}^n \in A$ is a probability distribution indicating the affinity between region i at $T + 1$ and each region j at $t \leq T$. Then, by multiplying A with the projected feature matrix M_t , we can obtain an updated representation for each time slot t by selectively focusing on regions that are more similar to the contexts of region v_i at $T + 1$. By taking the sum of representations

for all P time slots, Eq.(10) generates a temporal representation for each channel, denoted by \mathbf{M}_{S_1} , \mathbf{M}_{S_2} , \mathbf{M}_{S_3} and \mathbf{M}_{S_4} .

After obtaining the channel-wise representations, we merge all information into a unified spatiotemporal representation by sharing another self-attention unit across all four channels:

$$\mathbf{M}'_T = \sum_{\mathbf{M}_S \in \mathcal{S}'} \varrho\left(\frac{\mathbf{V}_{T+1} \mathbf{W}'_Q \cdot (\mathbf{M}_S \mathbf{W}'_K)^\top}{\sqrt{4d_e}}\right) \cdot \mathbf{M}_S \mathbf{W}'_V, \mathcal{S}' = \{\mathbf{M}_{S_1}, \mathbf{M}_{S_2}, \mathbf{M}_{S_3}, \mathbf{M}_{S_4}\}, \quad (11)$$

with weights $\mathbf{W}'_K, \mathbf{W}'_V \in \mathbb{R}^{4d_e \times 4d_e}$ and $\mathbf{W}'_Q \in \mathbb{R}^{d_o \times 4d_e}$ to learn. As such, the resulted matrix $\mathbf{M}'_T \in \mathbb{R}^{n \times 4d_e}$ is the final representation learned from all DDW graphs in $\{\mathbf{G}_t\}_{t=1}^T$. Essentially, \mathbf{M}'_T now encodes both the spatial and temporal information contained in DDW graphs up to time T , which can provide strong predictive signals for estimating the upcoming passenger demands.

3.4 Transferring Attention Layer

With the spatiotemporal representation \mathbf{M}'_T , we deploy a feed-forward layer to firstly compute an n -dimensional vector $\hat{\mathbf{d}}_{T+1} = [\hat{d}_1, \hat{d}_2, \dots, \hat{d}_n] \in \mathbb{R}^n$, where each element \hat{d}_i represents the total amount of outbound passenger demands (i.e., the out-degree of node v_i) at the next time slot $T+1$:

$$\hat{\mathbf{d}}_{T+1} = \sigma(\mathbf{M}'_T \mathbf{w} + \mathbf{b}), \quad (12)$$

with weight $\mathbf{w} \in \mathbb{R}^{4d_e}$ and bias $\mathbf{b} \in \mathbb{R}^n$ to learn. Intuitively, we derive $\hat{\mathbf{d}}_{T+1}$ to firstly capture the general trend and intensity of trip demands in each region, then distribute the total demands to different destinations in a fine-grained way. Meanwhile, it can also support traditional destination-unaware passenger demand prediction tasks [35, 40]. We denote this task as **Demand task** in this paper. In the following experiment, we conduct pretraining on this task before the formal training process so that we can obtain the accuracy results more quickly.

To map the total passenger demands \hat{d}_i from region node v_i to all n nodes, we calculate a transferring probability distribution $\{q_{ij}\}_{j=1}^n$ to indicate the likelihood of observing a passenger trip from v_i to each destination region v_j at the next time slot $T+1$. Specifically, as the i -th row $\mathbf{m}'_i \in \mathbf{M}'_T$ is a row vector carrying the spatiotemporal representation of node v_i , we calculate each probability $q_{ij} \in \{q_{ij}\}_{j=1}^n$ via the following attention mechanism:

$$q_{ij} = \frac{\exp(\text{AttentionNet}(\mathbf{m}'_i{}^\top, \mathbf{m}'_j{}^\top))}{\sum_{i=j}^n \exp(\text{AttentionNet}(\mathbf{m}'_i{}^\top, \mathbf{m}'_j{}^\top))}, \quad (13)$$

where the $\text{AttentionNet}(\cdot, \cdot)$ has the same structure as in Eq.(8) but uses a different set of parameters $\mathbf{a}' \in \mathbb{R}^{4d_e}$ and $\mathbf{W}'_a \in \mathbb{R}^{4d_e \times 4d_e}$. Finally, we can estimate every element in the next DDW graph $\hat{g}_{ij} \in \hat{\mathbf{G}}_{T+1}$ (which is denoted as the **OD task**) :

$$\hat{g}_{ij} = \hat{d}_i q_{ij}, \hat{g}_{ij} \in \hat{\mathbf{G}}_{T+1}, \hat{d}_i \in \hat{\mathbf{d}}_{T+1}. \quad (14)$$

Note that we only consider the start time of the passenger demand, that is, how many trip requests will generate between two nodes at the time slot $T+1$ no matter whether the trips will be finished in $T+1$.

3.5 Optimization Strategy

We formulate the overall loss function as follows:

$$\begin{aligned} \mathcal{L} &= \eta_d \mathcal{L}_d + \eta_o \mathcal{L}_o, \\ \mathcal{L}_d &= \text{SmoothL1Loss}(\hat{\mathbf{d}}_{T+1}, \mathbf{d}_{T+1}), \\ \mathcal{L}_o &= \text{SmoothL1Loss}(\hat{\mathbf{G}}_{T+1}, \mathbf{G}_{T+1}), \end{aligned} \quad (15)$$

where *SmoothL1Loss* [29] is a variant of the mean-squared-error loss which uses a squared term if the absolute element-wise error falls below 1 and an *L1* term otherwise; η_d, η_o are two hyperparameters balancing the importance of two tasks. The motivation of defining \mathcal{L} is to push our Gallat model to generate accurate predictions on both the overall demands ($\hat{\mathbf{d}}_{T+1}$) and the origin-destination demands ($\hat{\mathbf{G}}_{T+1}$). In addition, we conduct pretraining for our model on the Demand task's loss function \mathcal{L}_d firstly. Then with the relative accurate prediction of $\hat{\mathbf{d}}_{T+1}$, we train the model for the further prediction of $\hat{\mathbf{G}}_{T+1}$ (OD task) based on the pretrained model. All parameters are optimized with the Stochastic Gradient Descent (SGD) method. Specifically, we use Adam [15], a variant of SGD to optimize the parameters in our model.

3.6 Complexity Analysis

In this section, we analyze both the time and space complexity of Gallat.

3.6.1 Time Complexity. Putting away the convenient concatenation operation and weighted sum, the major computational cost of Gallat comes from the attention mechanisms used in our spatial, temporal, and transferring layers. For every node feature pair $(\mathbf{v}_i, \mathbf{v}_j)$, it takes $O(dd_e + 2d_e)$ time to compute a scalar attention score in Eq.(7). As there are n^2 possible combinations for n nodes, the total time complexity is $O(n^2dd_e + 2n^2d_e)$ for the computation in Eq.(8). At the same time, the self-attention modules in the temporal attention layer (i.e., Eq.(10) and Eq.(11)) consumes $O((P+1) \times (8nd_e^2 + nd_e d_v + 2n^2d_e))$ time to calculate. Similar to the spatial attention layer, Eq.(13) has the time complexity of $O(4n^2d_e^2 + n^2d_e)$. As $P, d_e,$ and d_v are typically small (see Section 4), the predominant factor in Gallat's time complexity is the total number of regions n . Also, as P, d_e, d_v and n are fixed in our model, the time complexity of Gallat is linearly associated with the scale of the data.

3.6.2 Space Complexity. The trainable parameters from the spatial, temporal and transferring attention layers are $\{\mathbf{W}_s, \mathbf{W}_a, \mathbf{a}\}, \{\mathbf{W}_S^K, \mathbf{W}_S^Q, \mathbf{W}_S^V, \mathbf{W}_K', \mathbf{W}_Q', \mathbf{W}_V'\},$ and $\{\mathbf{w}, \mathbf{b}, \mathbf{W}_a', \mathbf{a}'\},$ respectively. This results in a total parameter size of $(2dd_e + 2d_e) + (160d_e^2 + 20d_e d_v) + (16d_e^2 + 8d_e + n) = 176d_e^2 + 20d_e d_v + 2dd_e + 10d_e + n.$ Hence, the dominating term in the parameter size of Gallat is $176d_e^2,$ which has the space complexity of $O(d_e^2).$

4 EXPERIMENT

In this section, we conduct experiments on real-world datasets to showcase the advantages of Gallat in passenger demand prediction tasks. In particular, we aim to answer the following research questions via the experiments:

- RQ1:** How effectively does Gallat work on passenger demand prediction tasks?
- RQ2:** How does Gallat benefit from each component of the proposed model structure?
- RQ3:** How do the major hyperparameters affect the prediction performance of Gallat?
- RQ4:** What about the scalability of Gallat with the number of time slots/grids increasing?
- RQ5:** What's the effectiveness of the pretraining process on Demand task?
- RQ6:** Can Gallat learn useful mobility patterns from real data?

4.1 Datasets

We conduct experiments on two real-world datasets generated by Didi, which are both desensitized. Some similar datasets are publicly available¹. Table 2 summarizes the characteristics of two datasets. The first dataset is collected in Beijing covering the area within 6th Ring Road. The second dataset covers the urban area of Shanghai. Both datasets are collected from June to September in 2019.

¹<https://outreach.didichuxing.com/research/opendata/>

Table 2. A summary of datasets

dataset	Beijing	Shanghai
time span	4 months	4 months
total area	$53 \times 52 \text{ km}^2$	$57 \times 74 \text{ km}^2$
grid granularity	$2.65 \times 2.6 \text{ km}^2$	$2.86 \times 3.70 \text{ km}^2$
time slot granularity	1 hour	1 hour

We divide Beijing and Shanghai into 400 grids based on the granularities shown in Table 2 as the average time for a car to travel such distance is 5 minutes, which is a reasonable waiting time for passengers [43]. The DDW graphs on both datasets are constructed with 1-hour granularity. As the prediction results for passenger demands are mainly used as a reference for vehicle dispatching, so one-hour granularity can provide enough time for having the dispatching strategy operated in advance.

4.2 Baselines

To evaluate the performance of our model Gallat on demand prediction, we compare with the following baseline methods.

- **HA:** We adopt History Average to passenger demand prediction by calculating the mean of historical data at the same time slot of days and the same day of weeks.
- **LSTNet:** LSTNet [17] is a state-of-the-art time series prediction model, which combines both LSTM and CNN for spatiotemporal feature modelling.
- **GCRN:** The recently proposed GCRN [30] combines GCN with RNN to jointly identify spatial correlations and dynamic patterns.
- **GEML:** GEML [41] employs graph embedding in the spatial perspective and a LSTM-based multi-task Learning architecture in the temporal perspective to predict the passenger demands from one region to another.

4.3 Experimental Settings

We conduct experiments on passenger demand prediction settings, i.e., origin-destination demand prediction (denoted by “OD”) and origin-only demand prediction (denoted by “Demand”), which corresponds to our model output of $\hat{\mathbf{G}}_{T+1}$ and $\hat{\mathbf{d}}_{T+1}$, respectively. We measure the prediction accuracy with Mean Absolute Percentage Error (MAPE) and Mean Absolute Error (MAE) which have been widely used to evaluate the model performance in regression tasks:

$$MAPE = \frac{1}{n} \sum_{i=1}^n \left| \frac{\hat{y}_i - y_i}{y_i + 1} \right|, MAE = \frac{1}{n} \sum_{i=1}^n |\hat{y}_i - y_i|, \quad (16)$$

where n is the total number of instances, \hat{y}_i represents the predicted result and y_i represents the ground truth. In real-life applications, ride-hailing platforms concern more about the areas with more passenger demands. Regions having almost no passenger demand are less profitable and are paid less attention to. As a result, they only calculate the metrics for those records whose values are above some thresholds. In our experiments, we select three thresholds i.e., 0, 3, and 5 to calculate the metrics results which are termed as MAPE-0, MAPE-3, MAPE-5 and MAE-0, MAE-3, MAE-5, respectively. These are also used to evaluate the demand prediction on Didi platform now.

In experiments, we leave out the last two weeks of each dataset as the test set and the rest is training set. The last 10% of the training set is used for validation. We implement Gallat with Pytorch 1.5.0 on Python 3.8. When training Gallat, we use the Demand task to do pre-training first,

Table 3. Results of Different Methods-Beijing

Task	Method	Beijing					
		MAPE-0	MAPE-3	MAPE-5	MAE-0	MAE-3	MAE-5
OD	HA	2.7454	3.0059	3.1332	13.3953	39.7657	54.0634
	LSTNet	2.9443	4.3750	6.7874	14.8374	42.4918	95.2971
	GCRN	0.8347	0.9549	0.9693	5.0278	15.7346	23.3819
	GEML	0.8736	0.9244	0.9832	5.4396	12.6831	24.9918
	Gallat	0.7283	0.8465	0.8896	2.6781	3.4139	6.2347
Demand	HA	4.1315	3.7744	3.7077	512.7970	564.1135	593.6073
	LSTNet	12.5007	7.0283	5.3786	1329.3238	1589.1176	1608.4531
	GCRN	10.1060	4.1456	3.1136	127.3906	134.4935	148.2324
	GEML	0.8710	0.7671	0.7232	24.7852	29.3469	32.5521
	Gallat	0.6902	0.3904	0.3613	17.8332	20.0048	23.9004

Table 4. Results of Different Methods-Shanghai

Task	Method	Shanghai					
		MAPE-0	MAPE-3	MAPE-5	MAE-0	MAE-3	MAE-5
OD	HA	2.6416	2.8522	2.9670	18.5351	53.3798	71.8696
	LSTNet	3.8422	4.6471	7.7677	28.1293	87.2351	112.3874
	GCRN	0.8714	0.9678	0.9783	4.1634	12.2219	16.4002
	GEML	0.8922	0.9210	0.9792	6.0167	12.3469	15.9975
	Gallat	0.6813	0.8752	0.9143	3.6138	5.3497	8.6622
Demand	HA	3.7065	3.4005	3.3711	414.8688	489.3267	522.7588
	LSTNet	15.9938	5.0623	4.6083	625.9973	688.1231	745.8227
	GCRN	8.1710	3.3146	2.4972	143.7841	149.9170	153.6679
	GEML	1.0220	0.7297	0.6832	37.4469	41.0042	49.6711
	Gallat	0.6899	0.4109	0.3815	21.3526	24.7359	29.1875

which can relieve the data sparsity problem and speed the training process. The default values of batch size, epoches, embedding dimension d_e , historical time slots P , and loss weights (η_d, η_o) are set as 20, 200, 16, 7 and (0.8, 0.2).

4.4 Effectiveness Analysis (RQ1)

Table 3 and Table 4 shows the results of state-of-the-art methods and Gallat under MAPE and MAE above thresholds on the test set. For the comparison with other models, we make the following observations from these two tables:

- It clearly shows that the results of LSTNet and GCRN on Demand task are even worse than HA while they are doing better on OD task. GEML and Gallat show stable performance on both tasks. It may be because LSTNet and GCRN just focus on single task in their model structure and GEML and Gallat both involve the two tasks in their design.
- Methods tailored for graph-structured data (GCRN, GEML, Gallat) achieve better overall performance on OD task. It might prove that it's a better choice to model the passenger mobility prediction as a graph-based problem so that the complicated interactions between nodes can be fully captured. And in all of them, Gallat takes a more sufficient consideration on the graph representation, which tends to be the main reason that Gallat outperforms other spatiotemporal models.

Table 5. Results of Different Variants-Beijing

Task	Method	Beijing					
		MAPE-0	MAPE-3	MAPE-5	MAE-0	MAE-3	MAE-5
OD	Gallat-S1	0.7728	0.9082	0.9347	3.8855	11.6697	15.7926
	Gallat-S2	0.7497	0.8689	0.9050	3.4523	10.2289	13.8688
	Gallat-S3	0.9534	0.8689	0.9049	3.5206	10.4229	14.1817
	Gallat-S4	0.7421	0.8846	0.9135	3.4258	10.2555	13.8887
	Gallat-S5	0.7598	0.7712	0.9462	3.3208	8.7657	11.6541
	Gallat	0.7283	0.8465	0.8896	2.6781	3.4139	6.2347
Demand	Gallat-S1	2.2931	1.1786	0.9723	52.5624	55.6956	57.5813
	Gallat-S2	0.7637	0.4291	0.3641	25.0391	26.4881	27.4193
	Gallat-S3	1.0001	0.5030	0.4109	26.5299	27.7005	28.4539
	Gallat-S4	1.0748	0.4858	0.3925	24.7973	25.8946	26.6563
	Gallat-S5	0.9714	0.4730	0.3810	24.3334	25.4282	26.1744
	Gallat	0.6902	0.3904	0.3613	17.8332	20.0048	23.9004

Table 6. Results of Different Variants-Shanghai

Task	Method	Shanghai					
		MAPE-0	MAPE-3	MAPE-5	MAE-0	MAE-3	MAE-5
OD	Gallat-S1	0.8635	0.8945	0.9194	5.6163	16.0487	21.5877
	Gallat-S2	0.8458	0.8843	0.9093	5.1938	14.6175	19.5689
	Gallat-S3	0.8673	0.9164	1.1901	5.3672	15.0821	20.1670
	Gallat-S4	0.8450	0.8841	0.9091	5.1041	14.3365	19.2251
	Gallat-S5	0.8338	0.8780	0.9056	5.1784	12.8859	16.5776
	Gallat	0.6813	0.8752	0.9143	3.6138	5.3497	8.6622
Demand	Gallat-S1	4.8831	1.5453	1.1307	64.4367	70.1194	72.9258
	Gallat-S2	1.0183	0.4603	0.3899	27.3659	30.2024	31.4659
	Gallat-S3	1.3682	0.5138	0.4076	27.7591	31.3426	32.9075
	Gallat-S4	1.0572	0.4402	0.3614	23.3665	26.2928	27.6677
	Gallat-S5	0.9371	0.4248	0.3605	23.3078	26.0122	27.2486
	Gallat	0.6899	0.4109	0.3815	21.3526	24.7359	29.1875

- On Demand task, as the demand threshold increases the MAPE on Demand task is decreasing while MAE keeps increasing. One possible reason is that, the scale of the prediction targets in Demand task is larger than that in the OD task. Then, when we enlarge the threshold, the ground truth, i.e., the dominator of MAPE in Eq.(16) is increasing more significantly than the absolute error in the numerator. Furthermore, Gallat's advantage against baselines is larger on MAPE-5, which demonstrates that our model is highly accurate in prediction the passenger flow for popular regions.

4.5 Component Analysis (RQ2)

To validate the performance gain from each component of our model, we conduct an ablation study in which we change one component from Gallat each time to form a variant model. We implement the following variants of Gallat:

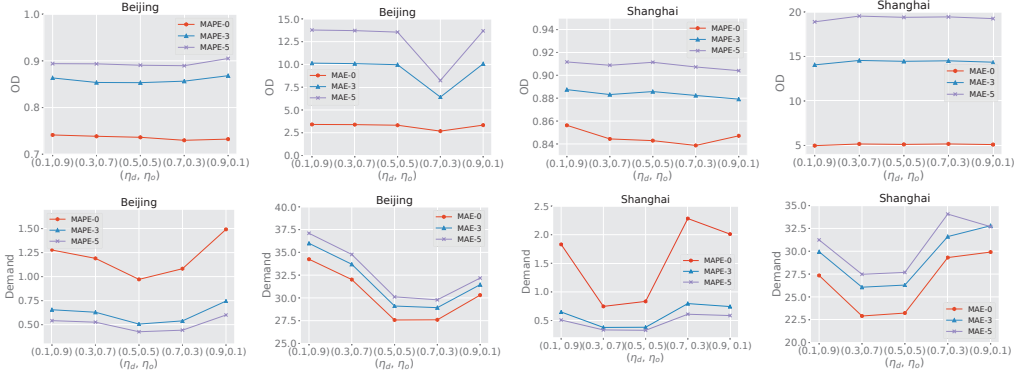


Fig. 5. Performance on different weights of task losses

- **Gallat-S1:** We use the existing method Graph Attention Networks (GATs) [38] to replace the spatial attention layer, which doesn't distinguish the forward and backward neighbors and ignores the geographical neighbors.
- **Gallat-S2:** We treat forward and backward neighbors as semantic neighbors like [41] in the spatial attention layer.
- **Gallat-S3:** We replace the attention-based aggregator in the spatial attention layer with the default mean aggregator as used in [10].
- **Gallat-S4:** We use a mean aggregator to replace the dot product attention in the temporal attention layer.
- **Gallat-S5:** We replace the transferring attention layer with a simple dense layer.

By comparing with the different variants of Gallat, a few observations can be obtained from Table 5 and Table 6:

- It is obvious that Gallat-S1 has the worst overall performance especially on the Demand task, which may indicate that the whole design of our spatial attention layer plays an important role in the overall performance of our model. And then the second worst is Gallat-S3, which means our attention-based aggregator in the spatial attention layer leads to significantly better effectiveness than the simple mean aggregator.
- The overall performance of Gallat-S2 is better than Gallat-S3, especially on the Shanghai dataset, indicating that the separation of forward and backward neighbor aggregation is necessary for providing more contexts for the prediction.
- The performance of Gallat-S4 is as inferior as Gallat-S2. Hence, we can tell that the attention mechanisms in both the temporal attention layer and transferring attention layer can help the Gallat selectively learn useful patterns for passenger demand prediction.
- Gallat-S5 shows 3 good results out of 24 ones which may indicate that the traditional dense layer has some advantages in learning transferring probabilities. However, Gallat-S5 is very unstable compared with other methods.

4.6 Hyperparameter Sensitivity Analysis (RQ3)

In this section, we discuss three important hyperparameters, that is, weights of task losses, i.e. η_d and η_o , and the number of historical time slots P in each channel. As hyperparameters are closely related to the performance of the model, we conduct experiments by varying their settings and record the new prediction results achieved. In what follows, we discuss the impact of these hyperparameters.

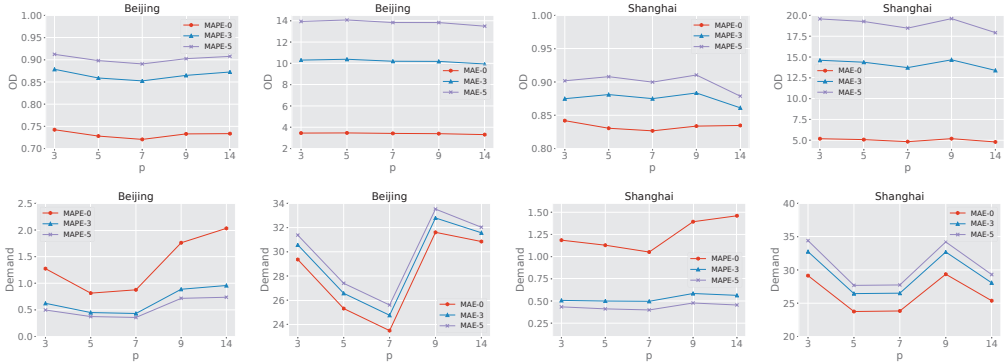


Fig. 6. Performance on different numbers of historical time slots

Loss Weights. As shown in Figure 5, we adjust the values of the loss weight pair (η_d, η_o) in both OD and Demand tasks. From the Figure, we can observe that:

- Under the same loss weights, the results on different datasets show different patterns. On Beijing dataset, the model gains better overall performance with $(\eta_d, \eta_o) = (0.7, 0.3)$. On Shanghai dataset, the weights around $(0.5, 0.5)$ shows more advantages. We suppose this is related to the different intrinsic features of two datasets like the scale and sparsity of the data. For instance, the sparsity of Beijing dataset is more severe than Shanghai's, and then the accurate prediction on OD passenger demands relies more on the accuracy of Demand task, so the model needs a relatively larger η_o .
- The Demand task is more sensitive to the loss weights than the OD Matrix task, especially on Shanghai dataset, which is possibly caused by the different demand distributions in different datasets.

Number of Historical Time Slots. Figure 6 depicts the variation trend of model's performance under different numbers of historical time slots P considered in each channel. Our findings are as follows:

- The results show that the performance of the model does not always improve with an increasing value of P . Also, we can see an obvious trend from Figure 6 that when we set P based on a periodic value like the number of days in a week (i.e., 7, 14, etc.), the model shows a better performance overall.
- Combining Figure 6 with Figure 5, Table 3 and Table 4, we can see that the results on Shanghai dataset is worse and more fluctuant than on Beijing dataset. This indicates that this dataset has more complex temporal patterns, thus being more sensitive to the hyperparameter P .

4.7 Scalability Analysis and Effectiveness of Pretraining

In order to testify the model's scalability and the effectiveness of pretraining, we conduct several groups of experiments on both datasets and the results are shown in Figure 7. In each group of experiments, except the variable parameter, the other parameters are set as default values following Section 4.3.

Scalability Analysis (RQ4). Figure 7(a) and 7(b) describe the training time cost. In the first group of experiment, we set the number of grids as 100 while in the second one, we utilize 4 months' data on both datasets. The summary of this part is as following:

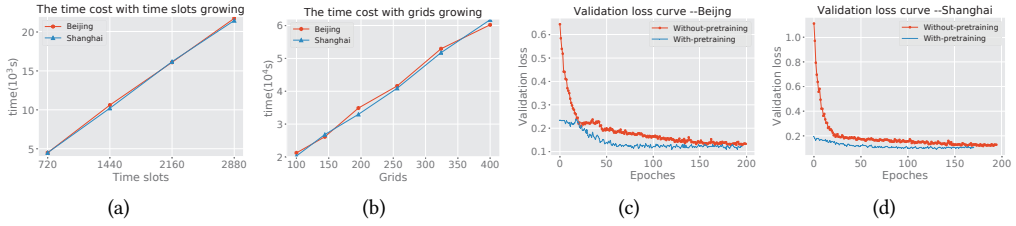


Fig. 7. The time cost and the validation loss curve of our model

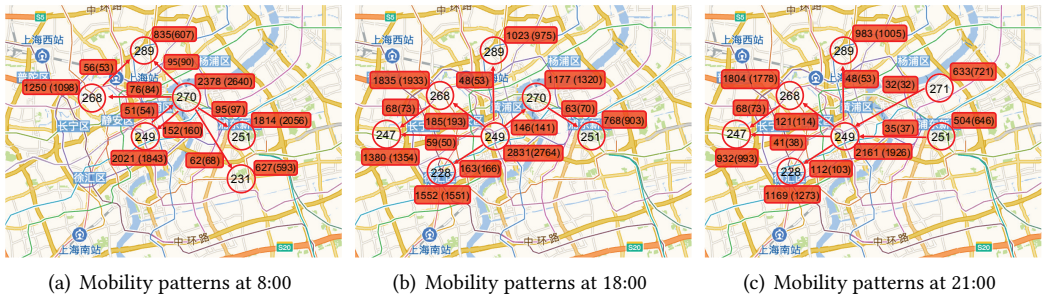


Fig. 8. The visualization of mobility patterns in Shanghai

- It is obvious that as the number of the time slots and grids increase, the time cost of the model training is almost growing linearly, especially the time cost with the growing number of time slots.
- The time cost curve with increasing grids is less strictly linear. The possible reason is that the number of grids affects not only the data size but also the number of different neighbors in the spatial part which brings more complex impact to the training time than simple increasing the data size .

Effectiveness of Pretraining (RQ5). Figure 7(c) and 7(d) show the validation loss under the conditions of with-pretraining and without-pretraining. We can see from the figures:

- The start loss of training process with pretraining is much lower than that without pretraining which means that the pretraining process would help fit the model on both tasks better.
- On both datasets, we can see that the pretraining offers faster convergence and a lower final loss, indicating that it is beneficial for our model.

4.8 Visualizing Learned Passenger Demand and Mobility Patterns (RQ6)

In order to better understand the latent patterns learned by Gallat, we use Figure 8 to visualize a part of passengers’ demand patterns of the most popular regions in Shanghai predicted by Gallat during three different time slots. The red circle marks a region node on the map with its ID. The red rectangles and the arrows illustrate how many passengers transfer from one node to another. The first value in the rectangle is the predicted result of our model while the one in the bracket is the corresponding ground truth. From Figure 8, we can draw the following observations:

- Figure 8(a) depicts the transferring relationship centered on node 270 at 8:00 am. As node 270 is a major residential area, it is the starting location for many people to leave home and march to several business districts and entertainment places, such as node 289 and 251, which cover a business district and the Shanghai Century Park, respectively.

- Figure 8(b) demonstrates the passenger mobility centered on node 249 which is a famous business district called Shanghai Xin Tian Di. Around 6:00 pm, a large amount of passengers leave this area to other residential or nightlife districts such as node 268 and node 228. There are also passengers going to node 247, which has a large train station and an airport.
- Figure 8(c) illustrates the transferring relationship centered on node 249 at 9:00 pm. Compared with Figure 8(a) and 8(b), it clearly shows that there are both passengers going to and leaving node 249. It may be because 249 also contains many nightlife venues like bars. There are also passengers travelling to node 247 to take night trains or flights.

5 RELATED WORK

This section introduces the state-of-the-art studies related to our problem. We classify them into three categories.

5.1 Sequence Based Prediction Problem

Basically, our problem is a sequence based prediction problem. There are already many existing studies in this field [2, 9, 12, 17, 23, 33, 35, 39, 40, 43–45, 47] which provide much inspiration for us. As the development of ride-hailing applications, we can collect more accuracy passenger demand data instead of traditional trajectory data from taxis to do research. Some studies [12, 23, 35, 39, 40, 43, 45, 47] have focused on passenger demand prediction via these kinds of data.

Tong et al. [35] put forward a unified linear regression model based on a distributed framework with more than 200 million features extracted from multi-source data to predict the passenger demand for each POI. Yao et al. [47] propose a deep multi-view spatial-temporal network framework to model both spatial and temporal relations. Specifically, their model consists of three views: temporal view (modelling correlations between future demand values with near time points via LSTM), spatial view (modelling local spatial correlation via local CNN), and semantic view (modelling correlations among regions sharing similar temporal patterns). Wang and Wei et al. [40, 43] present a combined model to predict the passenger demand in a region at the future time slot and the model catches the temporal trend with a novel parameter and fuses the spatial and other related features by ANN based on multi-source data. Lai et al. [17] propose a novel framework, namely Long- and Short-term Time-series network (LSTNet) which uses the Convolution Neural Network (CNN) and the Recurrent Neural Network (RNN) to extract short-term local dependency patterns among variables and to discover long-term patterns for time series trends. There are some other works [12, 23] based on bike sharing system. Hulot et al. [12] focus on predicting the hourly demand for demand rentals and returns at each station of the bike sharing system and then they focus on determining decision intervals which are often used by bike sharing companies for their online rebalancing operations. Liu et al. [23] develop a hierarchical station bike demand predictor which analyzes bike demands from functional zone level to station level. What's more, Zhang et al. [52, 53] design different models to predict the in-flow and out-flow of people in a given area, but still they ignore the transferring relationship between different areas.

All aforementioned methods have their own advantages but they model prediction problems as time series prediction problems and ignore the intrinsic connection and mobility between different areas or traffic interactions. Meanwhile, most of them need to draw support from sufficient multi-source data, which makes their model not that general and in low reproducibility.

5.2 Graph Based Prediction Problem

As traffic is based on networks consisting of lines and nodes, the traffic prediction can be naturally modeled into graph problems. Then graph-based methods [4–6, 11, 13, 14, 19–21, 24, 30–32, 41, 42, 50] can be used to solve them.

Deng et al. [4] define the traffic prediction based on the road network and given a series of road network snapshots, they propose a latent space model for road networks to learn the attributes of nodes in latent spaces which captures both topological and temporal properties. Li et al. [20] propose to model the traffic flow as a diffusion process on a directed graph and introduce diffusion convolutional recurrent neural network for traffic forecasting that incorporates both spatial and temporal dependency in the traffic flow. Wang et al. [41] design a grid-embedding based multi-task learning model where grid-embedding is designed to model the spatial relationships of different areas, and LSTM based multi-task learning focuses on modelling temporal attributes and alleviating the data sparsity through subtasks. Geng et al. [5] present the spatial-temporal multi-graph convolution network where they first encode the non-Euclidean pair-wise correlations among regions into multiple graphs and then explicitly model these correlations using multi-graph convolution. To utilize the global contextual information in modelling the temporal correlation, they further propose contextual gated recurrent neural network which augments recurrent neural network with a contextual-aware gating mechanism to re-weight different historical observations. Seo et al. [30] propose the Graph Convolutional Recurrent Network (GCRN), a deep learning model able to predict structured sequences of data. Precisely, GCRN is a generalization of classical recurrent neural networks (RNN) to data structured by an arbitrary graph. Jiang et al. [13] build an online system via RNN to conduct the next short-term mobility predictions by using currently observed human mobility data. Yu et al. [50] propose a novel deep learning framework, spatiotemporal graph convolutional networks, to tackle the time series prediction problem in traffic domain. Instead of applying regular convolutional and recurrent units, they formulate the problem on graphs and build the model with complete convolutional structures, which enables much faster training speed with fewer parameters.

These works have either of the following two problems. Firstly, although they define the traffic prediction as a graph-based problem, they fail to provide a good representation of the graph, and in other word, they don't fully use the attributes of the graph, i.e., dynamics, direction and weight. Secondly, most of them utilize the traditional transductive graph convolution, but it is not friendly to cold-start nodes, that is, nodes have no interaction with others.

5.3 Graph Representation Learning Method

Recently, the development of graph representation learning methods [1, 7, 10, 18, 25, 26, 28, 34, 36, 38, 48, 49, 51, 54–56] offer us some new thoughts to solve graph-based problems.

The well-known methods Deepwalk [28], Line [34] and node2vec [8] are both transductive and focused on static graphs. Hamilton et al. [10] propose an inductive methods to learn representation on large graphs, which solves the cold start problem but it still only focuses on spatial perspective and ignores the dynamic attribute of graphs. Veličković et al. [38] employ attention mechanism in the node embedding process which gives us many inspirations but unfortunately it is also based on static graphs. Trivedi et al. [36] build a novel modelling framework for dynamic graphs that posits representation learning as a latent mediation process bridging two observed processes namely dynamics of the network and dynamics on the networks. This model is further parameterized by a temporal-attentive representation network that encodes temporally evolving structural information into node representations, which in turn drives the nonlinear evolution of the observed graph dynamics. Zhang et al. [51] propose a new network architecture, gated attention networks (GaAN). Unlike the traditional multi-head attention mechanism, which equally consumes all attention heads, GaAN uses a convolutional sub-network to control each attention head's importance. These two studies above both propose novel frameworks over dynamic graphs but they don't support the directed and weighted attributes.

Goyal et al. [7] present an efficient algorithm DynGEM based on recent advances in deep auto-encoders for graph embeddings. The major advantages of DynGEM include: the embedding is stable over time; it can handle growing dynamic graphs; and it has better running time than using static embedding methods on each snapshot of a dynamic graph. Ma et al. [26] propose a Deeply Transformed High-order Laplacian Gaussian Process (DepthLGP) method to infer embeddings for out-of-sample nodes in dynamic graphs. DepthLGP combines the strength of nonparametric probabilistic modelling and deep learning. However, these two works only focus on the representation learning over dynamic and weighted graphs but they neglect the directions of edges.

6 CONCLUSION

In this paper, we define the passenger demand prediction problem in a new perspective, which is based on dynamic, directed and weighted graphs. To tackle this problem, we design a spatial-temporal attention network, Gallat, which includes spatial attention layer, temporal attention layer and transferring attention layer. In the spatial perspective, the spatial attention layer mimics the message passing process to formulate representation learning for each node by aggregating the information of all its neighbors. In this process, we add pre-weighted functions for three kinds of neighbors and utilize the attention mechanism to calculate the importance of different neighbors. In the temporal perspective, the temporal attention layer combines the learned representation of historical time slots and different channels via self-attention. Finally, we predict the passenger demand within an area first, and learn a transferring probability via attention mechanism to obtain the final passenger mobility in the future time slots. We conduct extensive experiments to evaluate our model, which demonstrates that our model significantly outperforms all the baselines.

ACKNOWLEDGMENTS

This work is luckily supported by the National Key Research & Development Program of China (2016YFB1000103) and Australian Research Council (Grant No.DP190101985, DP170103954).

REFERENCES

- [1] Hongxu Chen, Hongzhi Yin, Tong Chen, Quoc Viet Hung Nguyen, Wen Chih Peng, and Xue Li. 2019. Exploiting Centrality Information with Graph Convolutions for Network Representation Learning. In *2019 IEEE 35th International Conference on Data Engineering (ICDE)*. 590–601.
- [2] Tong Chen, Hongzhi Yin, Quoc Viet Hung Nguyen, Wen Chih Peng, Xue Li, and Xiaofang Zhou. 2020. Sequence-aware factorization machines for temporal predictive analytics. In *Proceedings - 2020 IEEE 36th International Conference on Data Engineering, ICDE 2020*. 1405–1416.
- [3] Zhiyong Cui, Kristian Henrickson, et al. 2018. Traffic Graph Convolutional Recurrent Neural Network: A Deep Learning Framework for Network-Scale Traffic Learning and Forecasting. *ICLR* (2018).
- [4] Dingxiong Deng et al. 2016. Latent space model for road networks to predict time-varying traffic. *SIGKDD* (2016).
- [5] Xu Geng, Yaguang Li, et al. 2019. Spatiotemporal multi-graph convolution network for ride-hailing demand forecasting. *AAAI* (2019).
- [6] Yongshun Gong, Zhibin Li, Jian Zhang, Wei Liu, Yu Zheng, and Christina Kirsch. 2018. Network-wide Crowd Flow Prediction of Sydney Trains via customized Online Non-negative Matrix Factorization. (2018).
- [7] Palash Goyal, Nitin Kamra, Xinran He, and Yan Liu. 2018. Dyngem: Deep embedding method for dynamic graphs. *arXiv preprint* (2018).
- [8] Aditya Grover and Jure Leskovec. 2016. node2vec: Scalable feature learning for networks. *SIGKDD* (2016).
- [9] Lei Guo, Hongzhi Yin, Qinyong Wang, Tong Chen, Alexander Zhou, and Nguyen Quoc Viet Hung. 2019. Streaming Session-Based Recommendation. In *Proceedings of the 25th ACM SIGKDD International Conference on Knowledge Discovery and Data Mining (KDD '19)*. 1569–1577.
- [10] Will Hamilton, Zhitao Ying, et al. 2017. Inductive representation learning on large graphs. *NIPS* (2017).
- [11] Jilin Hu, Bin Yang, Chenjuan Guo, Christian S Jensen, and Hui Xiong. 2020. Stochastic origin-destination matrix forecasting using dual-stage graph convolutional, recurrent neural networks. *ICDE* (2020).
- [12] Pierre Hulot, Daniel Aloise, and Sanjay Dominik Jena. 2018. Towards Station-Level Demand Prediction for Effective Rebalancing in Bike-Sharing Systems. *SIGKDD* (2018).

- [13] Renhe Jiang, Xuan Song, et al. 2018. DeepUrbanMomentum: An Online Deep-Learning System for Short-Term Urban Mobility Prediction. *AAAI* (2018).
- [14] Woojeong Jin, Meng Qu, Xisen Jin, and Xiang Ren. 2020. Recurrent Event Network: Autoregressive Structure Inference over Temporal Knowledge Graphs. In *Proceedings of the 2020 Conference on Empirical Methods in Natural Language Processing (EMNLP)*.
- [15] Diederik P Kingma and Jimmy Ba. 2014. Adam: A method for stochastic optimization. *arXiv preprint* (2014).
- [16] Thomas N Kipf and Max Welling. 2017. Semi-supervised classification with graph convolutional networks. *ICLR* (2017).
- [17] Guokun Lai, Wei-Cheng Chang, Yiming Yang, et al. 2018. Modeling long-and short-term temporal patterns with deep neural networks. *SIGIR* (2018).
- [18] Jianxin Li, Taotao Cai, Ke Deng, Xinjue Wang, Timos Sellis, and Feng Xia. 2020. Community-diversified influence maximization in social networks. *Information Systems* 92 (2020), 101522.
- [19] Lei Li, Kai Zheng, Sibowang, and Xiaofang Zhou. 2018. Go Slow to Go Fast: Minimal On-Road Time Route Scheduling with Parking Facilities Using Historical Trajectory. *The VLDB Journal* 27 (2018), 321–345.
- [20] Yaguang Li, Rose Yu, Cyrus Shahabi, and Yan Liu. 2018. Diffusion convolutional recurrent neural network: Data-driven traffic forecasting. *ICLR* (2018).
- [21] Wenwei Liang and Wei Zhang. 2020. Learning Social Relations and Spatiotemporal Trajectories for Next Check-in Inference. *IEEE Transactions on Neural Networks and Learning Systems* (2020), 1–11.
- [22] Binbing Liao, Jingqing Zhang, et al. 2018. Deep sequence learning with auxiliary information for traffic prediction. *SIGKDD* (2018).
- [23] Junming Liu, Leilei Sun, et al. 2017. Functional zone based hierarchical demand prediction for bike system expansion. *SIGKDD* (2017).
- [24] Lingbo Liu, Zhilin Qiu, Guanbin Li, Qing Wang, Wanli Ouyang, and Liang Lin. 2019. Contextualized Spatial–Temporal Network for Taxi Origin-Destination Demand Prediction. *IEEE TITS* (2019).
- [25] Zhijun Liu, Chao Huang, Yanwei Yu, Peng Song, Baode Fan, and Junyu Dong. 2020. Dynamic Representation Learning for Large-Scale Attributed Networks. In *Proceedings of the 29th ACM International Conference on Information and Knowledge Management (CIKM)*. 1005–1014.
- [26] Jianxin Ma, Peng Cui, and Wenwu Zhu. 2018. DepthLGP: learning embeddings of out-of-sample nodes in dynamic networks. *AAAI* (2018).
- [27] Andriy Mnih and Geoffrey E Hinton. 2009. A scalable hierarchical distributed language model. In *NIPS*.
- [28] Bryan Perozzi, Rami Al-Rfou, et al. 2014. Deepwalk: Online learning of social representations. *SIGKDD* (2014).
- [29] Girshick Ross. 2015. Fast-rnn. In *ICCV*.
- [30] Youngjoo Seo, Michaël Defferrard, et al. 2018. Structured sequence modeling with graph convolutional recurrent networks. *ICONIP* (2018).
- [31] Hongzhi Shi, Quanming Yao, Qi Guo, Yaguang Li, Lingyu Zhang, Jieping Ye, Yong Li, and Yan Liu. 2020. Predicting Origin-Destination Flow via Multi-Perspective Graph Convolutional Network. *ICDE* (2020).
- [32] Han Su, Guanglin Cong, Wei Chen, Bolong Zheng, and Kai Zheng. 2019. Personalized Route Description Based on Historical Trajectories. *CIKM* (2019), 79–88.
- [33] Han Su, Shuncheng Liu, Bolong Zheng, Xiaofang Zhou, and Kai Zheng. 2020. A Survey of Trajectory Distance Measures and Performance Evaluation. *The VLDB Journal* 29 (2020), 3–32.
- [34] Jian Tang, Meng Qu, et al. 2015. Line: Large-scale information network embedding. *WWW* (2015).
- [35] Yongxin Tong et al. 2017. The simpler the better: a unified approach to predicting original taxi demands based on large-scale online platforms. *SIGKDD* (2017).
- [36] Rakshit Trivedi, Mehrdad Farajtabar, Prasenjeet Biswal, and Hongyuan Zha. 2019. DyRep: Learning Representations over Dynamic Graphs. *ICLR* (2019).
- [37] Ashish Vaswani, Noam Shazeer, Niki Parmar, Jakob Uszkoreit, Llion Jones, Gomez, et al. 2017. Attention is all you need. *NIPS* (2017).
- [38] Petar Veličković, Guillem Cucurull, et al. 2017. Graph attention networks. *arXiv preprint* (2017).
- [39] Dong Wang, Wei Cao, Jian Li, et al. 2017. DeepSD: Supply-demand prediction for online car-hailing services using deep neural networks. *ICDE* (2017).
- [40] Yuandong Wang, Xuelian Lin, et al. 2019. A Unified Framework with Multi-source Data for Predicting Passenger Demands of Ride Services. *TKDD* (2019).
- [41] Yuandong Wang, Hongzhi Yin, Hongxu Chen, Tianyu Wo, et al. 2019. Origin-destination matrix prediction via graph convolution: a new perspective of passenger demand modeling. *SIGKDD* (2019).
- [42] Yuandong Wang, Hongzhi Yin, Tong Chen, Chunyang Liu, Ben Wang, Tianyu Wo, and Jie Xu. 2021. Gallat: A Spatiotemporal Graph Attention Network for Passenger Demand Prediction. In *2021 IEEE 37th International Conference on Data Engineering (ICDE)*.

- [43] Hua Wei, Yuandong Wang, et al. 2016. Zest: a hybrid model on predicting passenger demand for chauffeured car service. *CIKM* (2016).
- [44] Feng Xia, Jinzhong Wang, Xiangjie Kong, Zhibo Wang, Jianxin Li, and Chengfei Liu. 2018. Exploring Human Mobility Patterns in Urban Scenarios: A Trajectory Data Perspective. *IEEE Communications Magazine* 56, 3 (2018), 142–149.
- [45] Saijun Xu, Ruoqian Zhang, Wanjun Cheng, and Jiajie Xu. 2020. MTLM: a multi-task learning model for travel time estimation. *Geoinformatica* (2020).
- [46] Andy Yuan Xue, Jianzhong Qi, Xing Xie, Rui Zhang, Jin Huang, and Yuan Li. 2015. Solving the data sparsity problem in destination prediction. *VLDBJ* (2015).
- [47] Huaxiu Yao, Fei Wu, Jintao Ke, Xianfeng Tang, et al. 2018. Deep multi-view spatial-temporal network for taxi demand prediction. *AAAI* (2018).
- [48] Hongzhi Yin, Qinyong Wang, Kai Zheng, Zhixu Li, Jiali Yang, and Xiaofang Zhou. 2019. Social influence-based group representation learning for group recommendation. *ICDE* (2019).
- [49] Hongzhi Yin, Weiqing Wang, Hao Wang, Ling Chen, and Xiaofang Zhou. 2017. Spatial-Aware Hierarchical Collaborative Deep Learning for POI Recommendation. *IEEE Transactions on Knowledge and Data Engineering* 29, 11 (2017), 2537–2551.
- [50] Bing Yu, Haoteng Yin, et al. 2018. Spatio-temporal graph convolutional networks: A deep learning framework for traffic forecasting. *IJCAI* (2018).
- [51] Jiani Zhang, Xingjian Shi, Junyuan Xie, Hao Ma, Irwin King, and Dit-Yan Yeung. 2018. Gaan: Gated attention networks for learning on large and spatiotemporal graphs. *arXiv preprint* (2018).
- [52] Junbo Zhang, Yu Zheng, and Dekang Qi. 2017. Deep spatio-temporal residual networks for citywide crowd flows prediction. *AAAI* (2017).
- [53] Junbo Zhang, Yu Zheng, Junkai Sun, and Dekang Qi. 2020. Flow Prediction in Spatio-Temporal Networks Based on Multitask Deep Learning. *TKDE* (2020).
- [54] Yan Zhao, Shuo Shang, Yu Wang, Bolong Zheng, Quoc Viet Hung Nguyen, and Kai Zheng. 2018. REST: A Reference-based Framework for Spatio-temporal Trajectory Compression. *KDD* (2018), 2797–2806.
- [55] Kai Zheng, Yan Zhao, Defu Lian, Bolong Zheng, Guanfeng Li, and Xiaofang Zhou. 2020. Reference-Based Framework for Spatio-Temporal Trajectory Compression and Query Processing. *IEEE Transactions on Knowledge and Data Engineering* 32, 11 (2020), 2227–2240.
- [56] Lekui Zhou, Yang Yang, et al. 2018. Dynamic network embedding by modeling triadic closure process. *AAAI* (2018).